Study of the aggregation behavior of Janus particles by coupling experiments and Brownian dynamics simulations

Khaoula Lebdioua, Manuella Cerbelaud, Anne Aimable, Arnaud Videcoq

Version of Record: https://www.sciencedirect.com/science/article/pii/S0021979720312108
Manuscript_56478071bfa1d35e0dde4eb235c56e98

Study of the aggregation behavior of Janus particles by coupling experiments and Brownian dynamics simulations

Khaoula Lebdioua, Manuella Cerbelaud*, Anne Aimable*, Arnaud Videcoq

Univ. Limoges, CNRS, IRCER, UMR 7315, F-87000 Limoges, France

Abstract

Hypothesis

New colloids such as inverse patchy particles or Janus particles are considered as smart building blocks in the development of innovative and performant materials. For example, the control of the self-assembly of oxide-based charged Janus particles is interesting for ceramic shaping. Thus, the synthesis of silica based Janus particles as well as a detailed study of their behavior in suspension are presented in this paper.

Experiments

Fluorescent silica particles are partially modified in surface by grafting amine groups using a Pickering emulsion route. Zeta potential measurements, sedimentation tests and confocal microscopy observations are carried out to analyze the aggregation of the obtained particles in aqueous suspension as a function of the patch size and of the pH. Brownian dynamics simulations are also performed to better understand the aggregate structures.

Findings

The aggregation of the synthesized silica-based Janus particles can be tuned by modifying the experimental parameters, and elongated or on the contrary more compact structures could be observed. This control of aggregation makes such particles promising to build new ceramic materials.

Keywords: Colloid; Aggregation; Inverse patchy particles; Brownian dynamics simulations; Confocal microscopy

*Corresponding author

Email addresses: manuella.cerbelaud@unilim.fr; Tel: +33 (0)5 87 50 23 47 (Manuella Cerbelaud), anne.aimable@unilim.fr; Tel: +33 (0)5 87 50 23 68 (Anne Aimable)

1. Introduction

Colloid science is crossing multiple scientific disciplines, such as food and nutrition, cosmetics, biology, soft matter, nanophysics, or nanomaterials [1]. Colloidal interactions depend on the surface chemistry and the chemical environment of the colloids, which both determine their surface charge, and their hydrophilic or hydrophobic properties. Researchers have addressed this field from a long time with both experimental and fundamental studies, as many real problems may be solved through a better understanding and control of colloidal interactions; for example aggregation in biological fluids, or clogging in industrial processes. To describe real systems with more accuracy (for example proteins often carry different surface charges), anisotropic particles with inhomogeneous surface properties have been studied. Various morphologies exist: Janus particles, which present two different hemispheres, or patchy particles, with one or several different chemical functions or materials present on a smaller fraction of the surface. These anisotropic particles are able to assemble in more complex structures to achieve original clusters, mimicking molecular or crystal arrangements at the colloidal scale [2, 3]. Their synthesis is a difficult task, even at a laboratory scale. Different strategies can be found in the literature [4]. They usually consist in masking an hemisphere, and then modify the free surface. For most methods, one of the limitations is the low production yield, as only one monolayer of colloids is disposed at one interface. In that context the use of Pickering emulsions is a promising approach which deals with much more particles by synthesis [5]. In this method, colloids are entrapped at the interface of and oil-in-water emulsion prepared at moderate temperature (50 - 70°C) in order to have a liquid oil phase, which solidifies during cooling at ambient temperature. Colloids surface can be modified by a chemical grafting, before being released by dissolving the oil (in general paraffin). Granicks group first prepared dipolar silica particles with an aminosilane introduced in solution [6], or in vapor-phase [7]. They showed how the silica surface available was directly controlled by the contact angle at the O/W interface and thus by the surfactant concentration [8]. Other authors have then extended this technique to produce fluorinated silica [9], to decorate silica sheets with gold nanoparticles [10], or to create a TiO_2 layer on silica [11] for catalytic applications.

In this paper, the Pickering emulsion synthesis has been selected to produce charged Janus particles, also called zwitterionic particles. These are anisotropic particles showing attractive

interactions between the patch and the unpatched surface, and repulsive interactions between similar patches and unmodified bodies. Such organic charged particles have been for example proposed as drug delivery carriers [12, 13]. Our goal is to present a comparative study with experimental and numerical results on inorganic charged Janus particles, in order to get a better understanding of their interactions, and to control their self-assembly in future applications. Some previous studies have already shown some comparisons between experimental suspensions and numerical simulations, for charged Janus particles for example [14]. Aggregation of two-patches inverse patchy colloids has been also studied in details experimentally and numerically by Bianchi et al. [15, 16]

First, the synthesis of Janus particles of fluorescent silica will be presented. Then different conditions of aggregation will be studied, by varying the size of the patch, as well as the surface charges by varying the pH. The aggregates formed will be observed directly in suspension by confocal microscopy. They will be compared to those obtained using Brownian dynamics simulations.

2. Experimental methods

2.1. Particles synthesis

In this study, the synthesis of silica Janus particles is obtained from fluorescent silica particles which are home-made. Then their surface is modified on only one part by aminopropyltriethoxysilane (APTES) to obtain zwitterionic particles. For that, a Pickering emulsion route as proposed by Hong *et al.* [6] is used. The different steps of the synthesis are described in the following, with the details of the chemicals used at each step.

Synthesis of fluorescent silica particles. Fluorescent silica particles are synthesized according to the protocol described in Reference 17. This modified Stöber synthesis follows two steps. First, a classical Stöber method is employed, in order to synthesize monodispersed and spherical submicronic silica particles, by adding tetraethyl orthosilicate (TEOS) (98%, Acros Organic) in a mixture of ethanol (absolute ethanol, BDH Prolabo), reverse osmosed water, and ammonia solution (NH_4OH 28%, Acros Organic). Then the fluorescent dye (here the fluorescein isothiocyanate isomer I 90% (FITC), emission: $\lambda_{max} = 525\,\mathrm{nm}$, Sigma-Aldrich) previously bonded with the aminopropyltriethoxysilane (APTES)(99%, Sigma Aldrich) is added. In a second step, a silica shell is grown by a dropwise addition of TEOS, in order to

cover and thus stabilize the fuorescent dye. Following this protocol presented in Reference 17, fluorescent core-shell silica particles, with a size of around 600 nm are obtained.

Pickering emulsions. In order to modify partially the fluorescent silica particles, it is necessary to hide a part of them. In this study, the particles are trapped in solid paraffin droplets as proposed in Reference 6. For that, Pickering emulsions are prepared with paraffin wax (Fisher Scientific), water and silica particles [18]. To obtain partially hydrophobic silica, particles were modified by didodecyldimethylammonium bromide (DDAB, Sigma Aldrich). 140 mg of silica particles are thus introduced in 14 mL of osmosed water with the DDAB. The suspensions are stirred at least 12 h to allow the DDAB adsorption on the silica particles. As already shown in References [8, 18] the quantity of DDAB fix the contact angle between the particle and the wax, and therefore the depth of penetration of silica particles in the wax droplets. By modifying the quantity of DDAB, the surface available for modification and therefore the patch size of the future Janus particles can be tuned. In the following, three different amounts of DDAB ($R = m_{DDAB}/m_{SiO2}$ with m_{DDAB} the DDAB mass and m_{SiO2} the silica mass) will be used: $R = 5 \times 10^{-4}$, 1×10^{-3} and 1.5×10^{-3}. Paraffin wax (1 g) was added in the DDAB-silica suspension to obtain a Pickering emulsion. The mixture is placed in a thermostated bath, and heated at 90°C, in order to bring the wax above its melting point. Emulsification is performed using Ultra Turrax. The speed of stirring was set at 19000 rpm during a short time (one minute). The emulsions are then removed from the bath to ensure the solidification of the stabilized wax droplets at room temperature. At this stage, silica particles are trapped on solid wax droplets embedded in water.

APTES grafting. Naturally, silica particles are negatively charged in aqueous suspensions. In order to have zwitterionic particles, the not hidden part of particles will be modified by grafting APTES. Generally, this grafting is performed in anhydrous solvents or in ethanol based solvents in order to better control the rate of grafting [19, 20, 21]. Indeed, in water, the APTES molecules can react with themselves limiting the grafting on silica [22, 23]. Many anhydrous solvents dissolve the wax and thus can not be used in this study. Moreover, it is known that ethanol can release silica particles from the solid wax droplets [8, 18] which makes this solvent also not suitable for this study. That is why, even if grafting is not well controlled, APTES will be grafted directly in water. Cuoq *et al.* have indeed shown that a good rate of APTES grafting can be also obtained in water [22]. In this study, APTES is

added in the cold suspensions under stirring. Stirring is maintained over 20 minutes. Then the emulsion is filtered on a Buchner funnel using 10 cm diameter Whatman Gr.541 filter paper and rinsed with deionized water. The solid wax droplets are then let to dry during 48 h at ambiant temperature.

Wax removal. The last stage of the synthesis consists in releasing the Janus particles from the wax droplets. For that, wax is dissolved using cyclohexane. To try to isolate only the synthesized Janus particles, after dissolution, the mixture was centrifuged at 3000 rpm and powder was obtained. However, it appeared that the obtained particles are mixed with small pieces of wax. Moreover, the obtained particles are found hydrophobic because DDAB is still adsorbed on them. Instead of centrifugation, a method using settling has been preferred. In order to detach the DDAB, a HCl solution at pH 4 has been added in the beaker avoiding swirling and stirred slowly over the night in order to avoid emulsification. After, the mixture is let to settle in a separatory funnel. The two immiscible phases are observed and with time, colloids settle from the upper cyclohexane phase to the lower HCl solution. In HCl, the particles are aggregated which facilitates their sedimentation. At the end, the settled colloids in HCl solution are less hydrophobic because they are not trapped at the interface. The aqueous phase is isolated and centrifuged at 3000 rpm. Powder is then dispersed an other time 24 h in HCL solution at pH 4 in order to remove all the remaining DDAB. After that, the powder is centrifuged, rinsed 4 times in osmosed water and dried at 50°C during 16 h. It has been verified that the obtained powders dispersed in water at a basic pH are not able to promote the formation of a wax in water emulsion, which proves that the DDAB has been removed from the particles.

2.2. Characterization techniques

Solid wax droplets are observed by scanning electron microscopy (SEM) on a SEM-Quanta FEG - 450. To avoid charging effects, a thin film of platinum is deposited onto samples. As proposed in References 8 and 18, SEM is used to determine the penetration depth of particles in the solid wax droplets. For that, the emulsions were rinsed by ethanol to remove the silica from the wax. By comparing the diameter of the voids left in the wax and the silica diameter, the penetration depth or the proportion of silica surface area taken up in the wax is evaluated.

Zeta potential is measured using a Zetasizer Nano ZS from Malvern. For that, suspensions of 0.3vol% are prepared in osmosed water and pH was adjusted with NaOH 0.1 M and HCl 0.1 M.

To check the Janus balance of the synthesized particles, suspensions composed of Janus particles and 25 nm silica particles (Ludox®TM50 supplied by Grace Davidson, United States) were made at 0.5vol%. For this purpose, the silica suspension was diluted by three and added to the Janus particle suspension. The pH of the mixture was adjusted to 5 by adding 0.1 M HCl. Under these conditions, the Janus particles were assumed to be zwitterionic and the negatively charged silica particles should adsorb on the positively charged portion of the Janus particles. A drop of suspension was then deposited on a sample holder and left to dry before being analyzed by SEM (LEO 1530 vp).

Aggregation is evaluated performing sedimentation tests. Suspensions are prepared with an amount of 1vol% of silica particle at different pH. After preparation, the suspensions are introduced into closed tubes and are allowed to settle. Analyses are performed after 24 h. The more stable the suspensions are, the lower the sediment heights will be.

Because silica particles are labeled by FITC, suspensions are observed by a confocal microscope LSM880 from Zeiss. Suspensions are deposited between slide and slip cover. Images are treated with ImageJ.

3. Simulation methods

Brownian dynamics simulations will be performed considering a 'raspberry' representation of the Janus particles. Details on this simulation technique can be found in Reference 24. To summarize, the surface of each spherical colloid is discretized by 92 beads (see Figure 3), which are used to calculate the electrostatic interaction between two colloids.

The interaction between Janus particles is modeled here trough a DLVO potential (Derjaguin, Landau, Verwey, Overbeek) [25, 26], which is the sum of two contributions: one attractive due to van der Waals interactions, and an electrostatic one due to the surface charges of the colloids. In this numerical study, the attractive interaction is applied as a central force and is expressed as:

$$V_{IJ}^{vdW} = -\frac{A_{IJ}}{6}\left[\frac{2a^2}{r_{IJ}^2-(2a)^2}+\frac{2a^2}{r_{IJ}^2}+\ln\left(\frac{r_{IJ}^2-(2a)^2}{r_{IJ}^2}\right)\right] \quad (1)$$

where A_{IJ} is the Hamaker constant, a is the radius of the Janus particles and r_{IJ} is the distance between the centers of the Janus particles I and J. Here $a = 300\,\text{nm}$ and $A_{IJ} = 4.6 \times 10^{-21}\,\text{J}$ [27]. The electrostatic interaction applied on a Janus particle is obtained by the sum of the electrostatic interactions applied on its beads, which are represented by a Hogg Healy Fuerstenau (HHF) potential [28]:

$$V_{ij}^{HHF_{bead}} = \pi\epsilon\frac{4a_b}{2}\left(\psi_i^2 + \psi_j^2\right)\left[\frac{2\psi_i\psi_j}{\psi_i^2 + \psi_j^2}\ln\left(\frac{1+\exp(-\kappa h_{ij})}{1-\exp(-\kappa h_{ij})}\right) + \ln\left(1-\exp(-2\kappa h_{ij})\right)\right] \quad (2)$$

where ψ_i is the surface potential of bead i, h_{ij} is the distance between the surfaces of the beads i and j, κ the inverse of Debye length ($\kappa = 10^8\,\text{m}^{-1}$) and a_b is the bead radius (here $a_b = 66.58\,\text{nm}$). As proposed in Reference 24, a factor 4 is used in the HHF expression, which allows to reproduce the behavior of suspensions, where heteroaggregation occurs. To avoid interpenetration of Janus particles at the contact, the attractive interactions are cut at -14k_BT and a linear repulsive potential is introduced as a central interaction when Janus particles are in contact.

Both the translational and the rotational motions of colloids are introduced in Brownian dynamics simulations, which are performed in a cubic box with periodic conditions. 1500 Janus particles are considered in each simulation. A volume fraction of 3vol% is used. Simulations have been performed with a time step of $10^{-7}\,\text{s}$. Results are analyzed at 10 s. Because of the large number of beads used in these simulations, simulations have been performed thanks to a parallelized home-made code developed for GPU (Graphics Processing Unit) calculations [29].

4. Results and discussion

4.1. Characterization of the synthesized Janus particles

As already mentioned, the quantity of DDAB used to prepare the wax-in-water Pickering emulsion determine the depth of silica penetration in the wax and thus the surface that can be modified by APTES. To quantify this surface, some silica particles were removed from the wax thanks to an ethanol rinse of the cold emulsions (see Supporting Information). By measuring the diameter of the indentations, the depth of penetration and therefore the surface area accessible for modification have been determined. Modified surface area proportions of $S = 95\%$, $S = 88\%$ and $S = 72\%$ have been obtained with the DDAB ratios $R = 5 \times 10^{-4}$,

1×10^{-3} and 1.5×10^{-3}, respectively.

In order to check that the APTES is grafted on the silica during the synthesis, zeta potential measurements have been performed on the synthesized Janus particles as reported in Figure 1a. In comparison, the zeta potential measured for the raw silica particles (S=0%) as well as the zeta potential of silica particles whose surface is totally grafted by APTES (S=100%) are also reported. It can be observed that the raw silica have a negative zeta potential over the whole pH range, whereas the totally grafted silica particles show an isoelectric point around pH=7.5. Below this pH the modified silica particles are positively charged, due to the protonation of the NH_2 groups of APTES, whereas above this pH they are negatively charged. For the Janus particles, zeta potential curves are found in between the curves for S=0% and S=100%, which is in agreement with partial particle coverage by APTES. In addition, the larger the modified area are, the closer the curves are to the one at S=100%. Measurements of zeta potentials are global measurements that do not account for the charge distribution on the surface of the particles. They only allow us to know which types of charges are in the majority. The partial modification of the particle surface was confirmed by SEM observations of suspensions prepared from Janus particles (S=72%) and silica nanoparticles at pH 5. Under these conditions, the silica nanoparticles adsorb only on the positive part of the Janus particles, leaving the other part of the particle empty. After drying, the SEM photos show such an arrangement (see Figure 1(c)).

For Janus particles, zeta potential curves are not sufficient to understand the aggregation of suspensions, since they do not account for the non-uniform distribution of charges on the surface. Positively charged particles can in fact aggregate through the presence of negatively charged patches. That is why, to understand the behavior of Janus particle suspensions and for their simulation, it is important to know the electric potential at the surface of each part of the particles as a function of the pH: the unmodified part called "silica" and the modified part called "APTES". We discuss this point in the following.

A reasonable hypothesis would be to consider that the potential of the unmodified part is that of the initial silica, $\psi_{silica} = \psi_{0\%}$ (the potential measured for $S = 0\%$), and that the potential of the modified part is that measured for the completely modified silica, $\psi_{APTES} = \psi_{100\%}$ (the potential measured for $S = 100\%$). At this point, at pH=7.5, we would expect that the suspension would not be stable since $\psi_{100\%}$ is close to 0, but sedimentation tests show on the

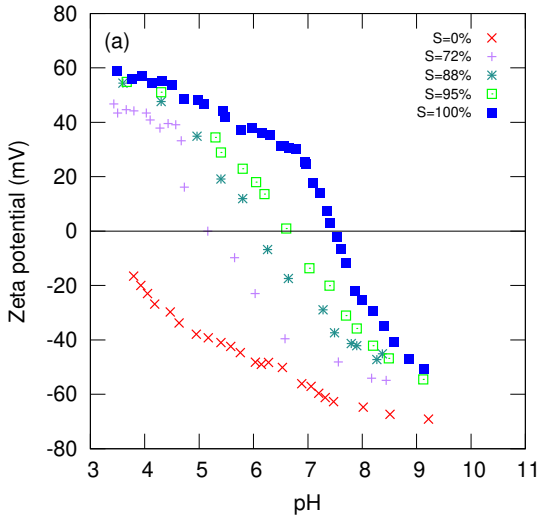

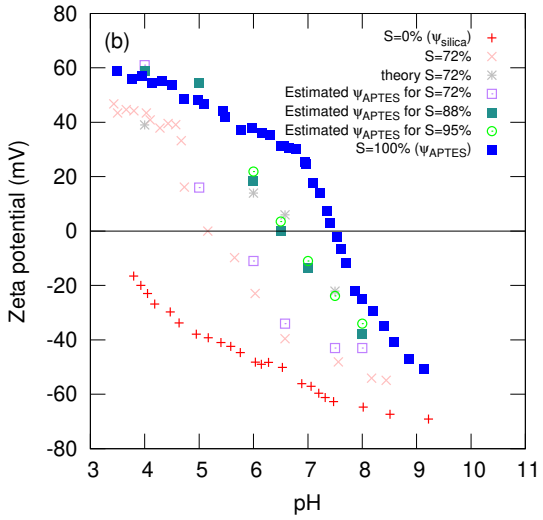

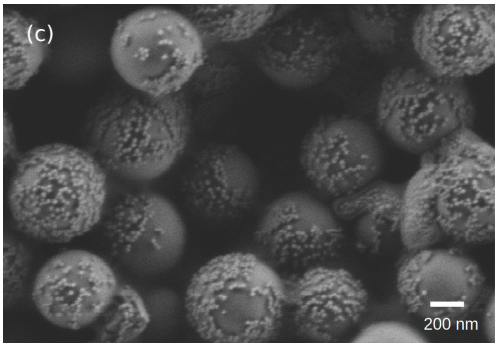

Figure 1: (a) Evolution of the experimental zeta potential of Janus particles as a function of the pH. By comparison, results obtained with raw silica particle ($S = 0\%$) and silica fully modified ($S = 100\%$) are reported. (b) Calculated surface potentials for $S = 72\%$ considering that the patch reacts as the raw silica and the unpatched part as the full APTES modified silica (theory S=72%). Calculated surface potentials of the APTES modified parts of Janus particles for S=72% (Estimated ψ_{APTES} for S=72%), S=88% (Estimated ψ_{APTES} for S=88%) and S=95% (Estimated ψ_{APTES} for S=95%). (c) SEM picture of a dried suspension prepared with Janus particles (S=72%) and Ludox TM50 silica nanoparticles at pH 5.

contrary that the suspension is stable at this pH. As surface potentials are not additive, it is necessary to go back to the number of charges carried by the particles to understand the overall behavior of the Janus particles. Knowing the surface potential, the following formula allows us to go up to the corresponding surface charge quantity [30]:

$$Z = 4\pi\epsilon\frac{k_BT}{ze^2}\kappa a^2\left[2\sinh\left(\frac{1}{2}\frac{ze\psi}{k_BT}\right)+\frac{4}{\kappa a}\tanh\left(\frac{1}{4}\frac{ze\psi}{k_BT}\right)\right], \quad (3)$$

where e is the elementary charge and z the electrolyte valence (here z=1). Thus, by using the surface proportion at $\psi_{0\%}$ and that at $\psi_{100\%}$, we can estimate the number of charges of the unmodified part Z_{silica} and that of the modified part Z_{APTES}, i.e., by summing up the total number of charges Z_T, and thus, by adjustment using equation 3, a theoretical surface potential ψ_{theo}. This estimate was made for Janus particles at $S = 72\%$ and the result is shown in Figure 1b. It is clearly observed that the calculated curve does not correspond to the measured one.

These two disagreements could be explained by a grafting rate of APTES, while the particles are embedded in the wax, lower than that obtained for completely uncovered particles ($S = 100\%$), without the wax. As already mentioned, the APTES grafting in water is difficult to control because of its self-reaction and moreover, in case of Pickering emulsions, the presence of different phases can also affect this grafting. This would mean that ψ_{APTES} is different from $\psi_{100\%}$ and lower.

Another hypothesis for estimating ψ_{APTES} is to deduce the total number of charges Z_T from the measured zeta potential, estimate the number of charges of the unmodified part Z_{silica} from the proportion of unmodified area and $\psi_{0\%}$ (ψ_{silica} is assumed to be equal to $\psi_{0\%}$), deduce Z_{APTES} from this and go back to ψ_{APTES} by fitting with equation 3.

These estimations, shown in Figure 1b, reveal that the surface potential of modified part may be lower than ψ_{APTES} in a pH range comprised in [5-7.5] for the case $S = 72\%$ and in a pH range of [6-7.5] for the cases $S = 88\%$ and 95%. For $S = 72\%$, the PCN of the modified part is estimated at 5.5 and thus at pH 7.5, both parts of particles may be negatively charged and thus suspension must be stable, which is in agreement with the previous sedimentation tests.

In the following, for each Janus particle, aggregation will be analyzed for three different pH. The first one, pH_a, corresponds to the case where the APTES modified surface is positively charged and the unmodified part is negatively charged. The second one, pH_n, corresponds

to a pH where the APTES surface modified has surface potential around 0. And the third one, pH_b, corresponds to the case where both parts of Janus particles are negatively charged. In the following, a pH in the range [4.5-5] is chosen as pH_a and a pH in the range [7.5-8] as pH_b whatever the size of the modified surface. Because of the difficulty to evaluate precisely the PCN of the modified part due the rough estimations used in the model as well as the experimental difficulties to obtain precise measurements of zeta potential near the isoelectric point, pH_n is chosen in a larger range [5.5-6.5]. At pH_n it is verified by sedimentation tests that the suspension aggregate and that, for higher pH, it becomes stable.

4.2. Study of Janus particles aggregation

Sedimentation tests are performed with colloidal suspensions prepared with a volume fraction of 1vol% for the different pH reported in the previous section. Figure 2 shows the results obtained at 24 h. Moreover, because particles are labeled with FITC, the suspensions are observed by confocal microscopy as also shown in Figure 2.

For pH_b, it is observed that all the suspensions are stable. The sediments are low and only individual particles are observed by microscopy. According to Figure 1, at pH_b both parts of Janus particles are negatively charged and thus aggregation of particles is unlikely. For pH_n, the raw silica is stable and negatively charged. However, this pH is near the isoelectric point of the APTES part of the Janus particles, which aggregate because of the van der Waals interactions. For Janus particles suspensions, higher sediment is observed in the sedimentation tubes and aggregates are clearly observed by confocal microscopy whatever the patch size. For this pH, few differences are observed according to the values of S.
As for pH_a, the totally modified particles (S=100%) and the raw silica particles (S=0%) are stable. Nevertheless, in case S=100%, particles are positively charged and in case S=0% particles are negatively charged (see Figure 1). For Janus particles suspensions at pH_a, the sediments are slightly lower than those obtained at pH_n. However they are higher than the sediments obtained at pH_b, which is explained by an aggregation of Janus particles in suspension. Aggregates are indeed observed by confocal microscopy. Differences in sizes and shapes are observed according to the values of S. At this pH, the patch and the unpatched parts of Janus particles are oppositely charged and aggregation can be explained by the attractions

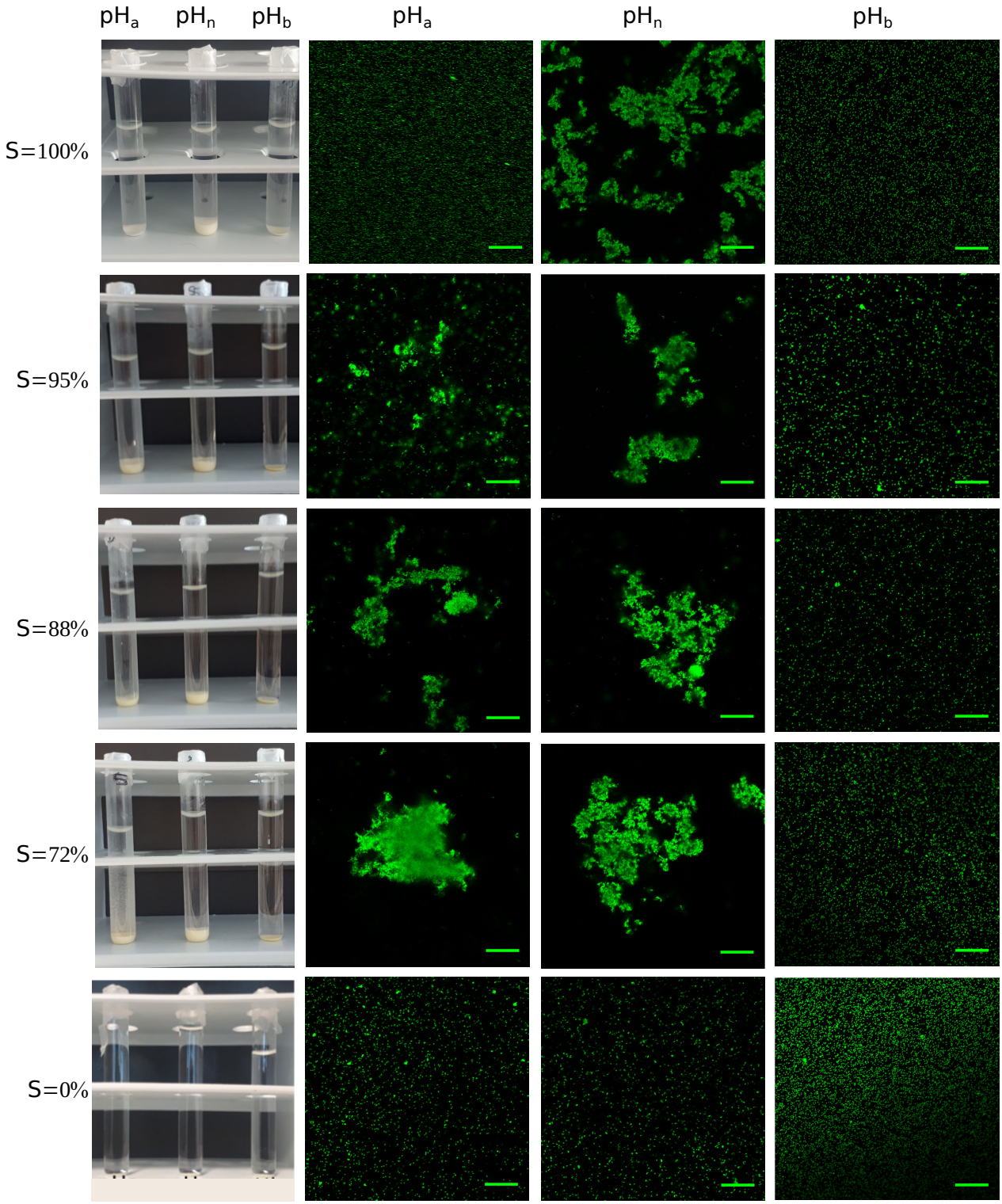

Figure 2: Picture of sedimentation test and corresponding confocal microscopy images for the different pH as a function of the size of the modified part of the Janus particles (S). The scale bar is for 20 μm.

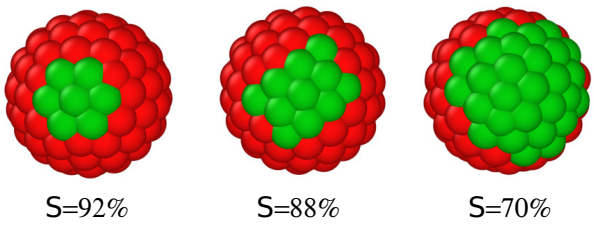

Figure 3: Snapshots of Janus particles used in Brownian dynamics simulations with their proportion of red surface area (corresponding to the APTES modified part).

	S=92%		S=88%		S=70%	
	ψ_{silica} (mV)	ψ_{APTES} (mV)	ψ_{silica} (mV)	ψ_{APTES} (mV)	ψ_{silica} (mV)	ψ_{APTES} (mV)
pH_a	-40	50	-40	50	-40	20
pH_n	-60	0	-60	0	-50	0
pH_b	-65	-25	-65	-35	-65	-45

Table 1: Summary of the different values of surface potentials (ψ) used in simulations.

between the two parts of Janus particles. For the largest patch (S=72%), confocal microscopy observations reveal that aggregates are compact (see Figure 2). To better understand the aggregation mechanisms in Janus particles suspensions, Brownian dynamics simulations have been used.

4.3. Brownian dynamics simulations of Janus particles aggregation

Figure 3 shows the Janus particles used in simulations. The green part corresponds to the unmodified part of silica particle and the red part corresponds to the APTES modified part. Patches are defined in order to fit with the experimental patch sizes. The surface potentials used in the HHF potential (Equation 2) are assimilated here to the surface potential of the raw silica (ψ_{silica}) for the unmodified part and to the estimated APTES surface potential (ψ_{APTES}) for the modified part. Table 1 summarizes the values of surface potential used in simulations.

For a comparison, a simulation has also been performed with particles without patch, which interact only via the van der Waals attraction (case where $S = 100\%$ at pH_n). Figures 4 and 5 show the results of simulations at $t = 10\,s$ for the different patch sizes. The aggregation kinetics as well as the evolution of the aggregate shape as a function of time are shown in Figure 6.

At pH_b, for all patch sizes, no aggregation is observed in the simulations in agreement with the experimental observations. Both parts of particles are negatively charged. Particles repel each other leading to stable suspensions.

At pH_a, for which the two parts of the Janus particles are oppositely charged, aggregation is observed regardless of S. Aggregates are formed by contacts between the modified and the unmodified parts of particles, which are oppositely charged (see Figure 5). However aggregate size and shape differ depending on S, as observed experimentally. Considering that an aggregate is composed of at least two colloids, the evolution of the number of aggregates as a function of time is plotted in Figure 6a. As already observed in Reference [24], the aggregation kinetics slows down when S increases. Thus, at the end of simulations, when S increases, the aggregate size decreases. This observation is in good agreement with the confocal microscopy pictures reported in Figure 2. To characterize the aggregate structure, the coordination number of aggregated particles is reported in Figure 6c. For all the values of S, at short times, this number is equal to 1. At this stage, aggregation starts with the formation of dimers, which increases the aggregate number as observed in Figure 6a and gives a coordination number equal to one for the particles in these aggregates. Then, when the number of aggregates decreases due to their coalescence, the coordination number increases. For $S = 70\%$, this number is around 6 at $t = 10\,\mathrm{s}$, which corresponds to quite compact aggregates as observed in Figure 5. However, it is around 2 or 3 for $S = 92\%$ and $S = 88\%$ respectively. In this case the aggregates are more linear (see Figure 5). To characterize the shape of aggregates, the asphericity parameter has been calculated, according to [31, 32]:

$$A_s = \frac{(\lambda_1 - \lambda_2)^2 + (\lambda_2 - \lambda_3)^2 + (\lambda_3 - \lambda_1)^2}{2(\lambda_1 + \lambda_2 + \lambda_3)^2} \tag{4}$$

with λ_1, λ_2 and λ_3 ($\lambda_1 \geq \lambda_2 \geq \lambda_3$) the eigenvalues of the radius of gyration tensor. For a sphere, A_s is equal to 0 and for a rod-like structure it is equal to 1. The evolution of A_s is reported in Figure 6e. At the beginning of simulations, whatever S, $A_s = 1$, which is explained by the dimers formed at this stage of aggregation. At $t = 10\,\mathrm{s}$, A_s is smaller when S decreases and therefore aggregates are more spherical. The analysis of the fractal dimensions (D_f), obtained as in Reference 24, confirms this observation. $D_f = 1.34 \pm 0.03$, 1.54 ± 0.03 and 1.96 ± 0.04 have indeed been found for $S = 92\%$, 88% and 70% respectively. An other important parameter for aggregated patchy particles is their mutual orientation

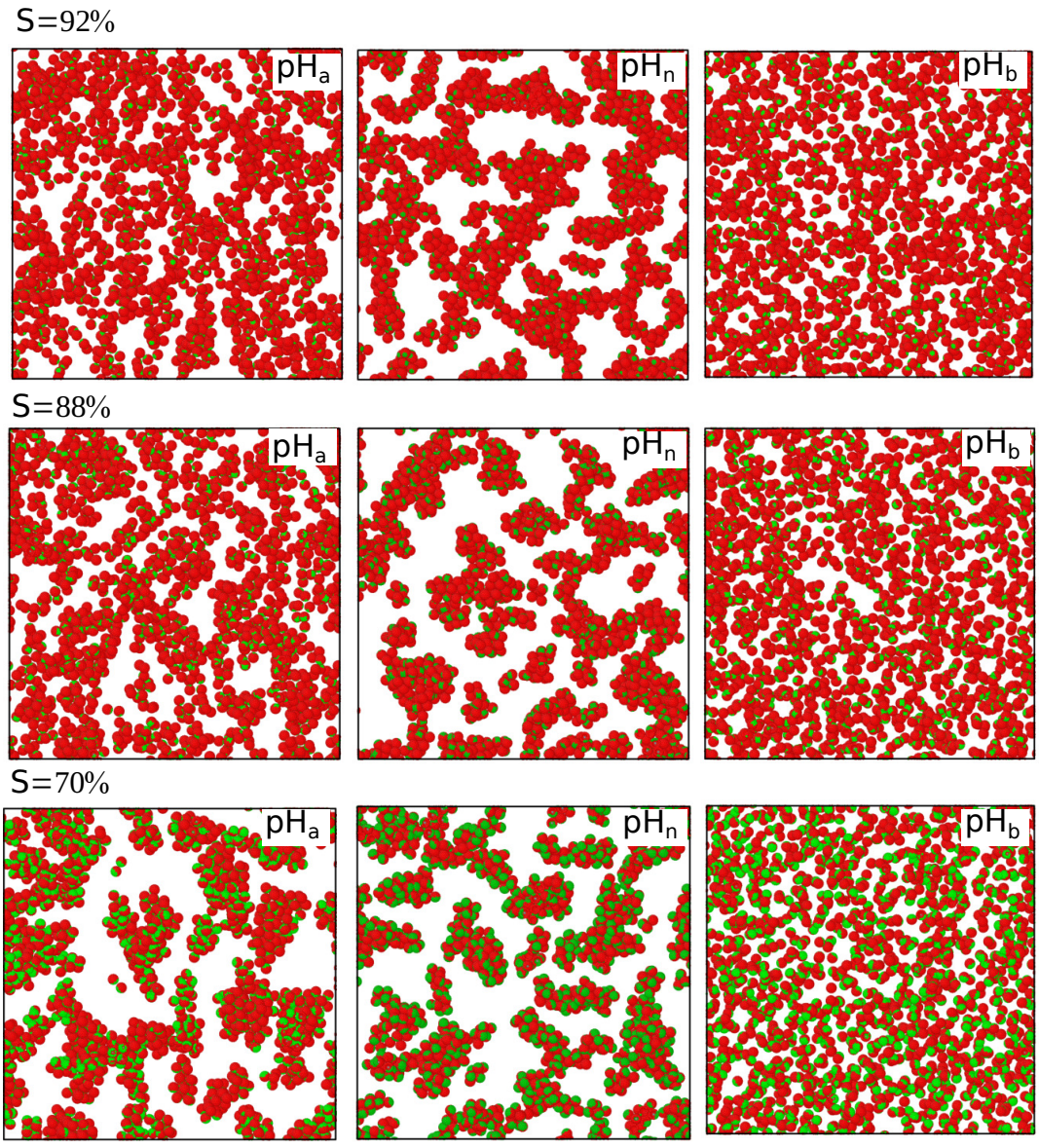

Figure 4: Snapshots of Brownian dynamics simulations obtained at $t = 10\,\mathrm{s}$ for the different pH as a function of the size of the unpatched part (APTES modified).

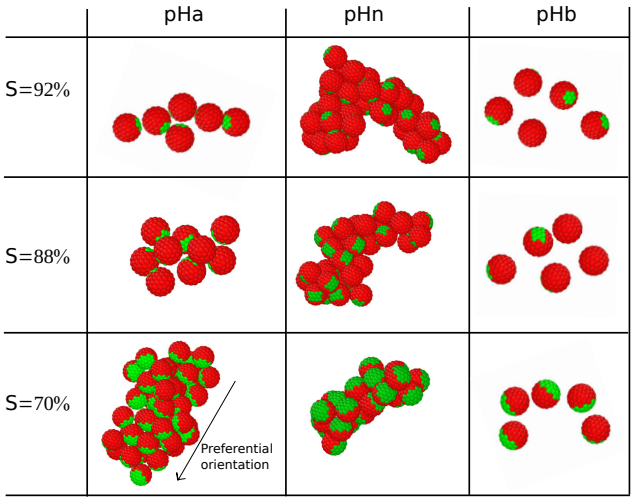

Figure 5: Snapshots of isolated aggregates extracted from the Brownian dynamics simulations performed with different pH and different sizes of the unpatched part (S). At pH_b no aggregate were formed.

in the aggregate. To characterize it, the nematic order parameter ($< P_2 >$) defined as in References [24, 33] is used. When all orientation vectors of neighboring particles are perfectly aligned, $< P_2 >$ is equal to 1. If all the neighboring particles are randomly oriented, $< P_2 >$ is null. An orthogonal orientation is traduced by a value of -0.5. The calculated values of $< P_2 >$ are small, which indicates that Janus particles are poorly oriented in the aggregates (see Figure 6g). However it is not zero. When $S = 70\%$, $< P_2 >$ becomes positive which corresponds to a beginning of alignment of particles in the same direction. This can be seen in Figure 4, where some aggregates appear completely red, which is due to the fact that the particles are more or less all oriented in the same direction. And in Figure 5, the main orientation of the particles is shown by the arrow next to the aggregate. However, for the higher S, $< P_2 >$ is negative, the unmodified parts are rather orthogonally oriented. All these observations are in agreement with previous observations from the literature [24, 34, 35]. At pH_a, the differences in particle orientation, aggregate size and structure, as a function of S, can be explained by the competition of attractive and repulsive electrostatic interactions between the two parts of the Janus particles. Depending on the size of the parts, these repulsions or attractions will be more or less important, leading to different morphologies.

At pH_n, simulations show a strong aggregation of particles whatever S, which is in agreement with the experimental observations (see Figure 2). Contacts in aggregates are obtained essentially between the modified parts or between the modified and unmodified parts. At this pH, there is not much difference in the aggregation kinetics for the different S (see Figure 6b). It

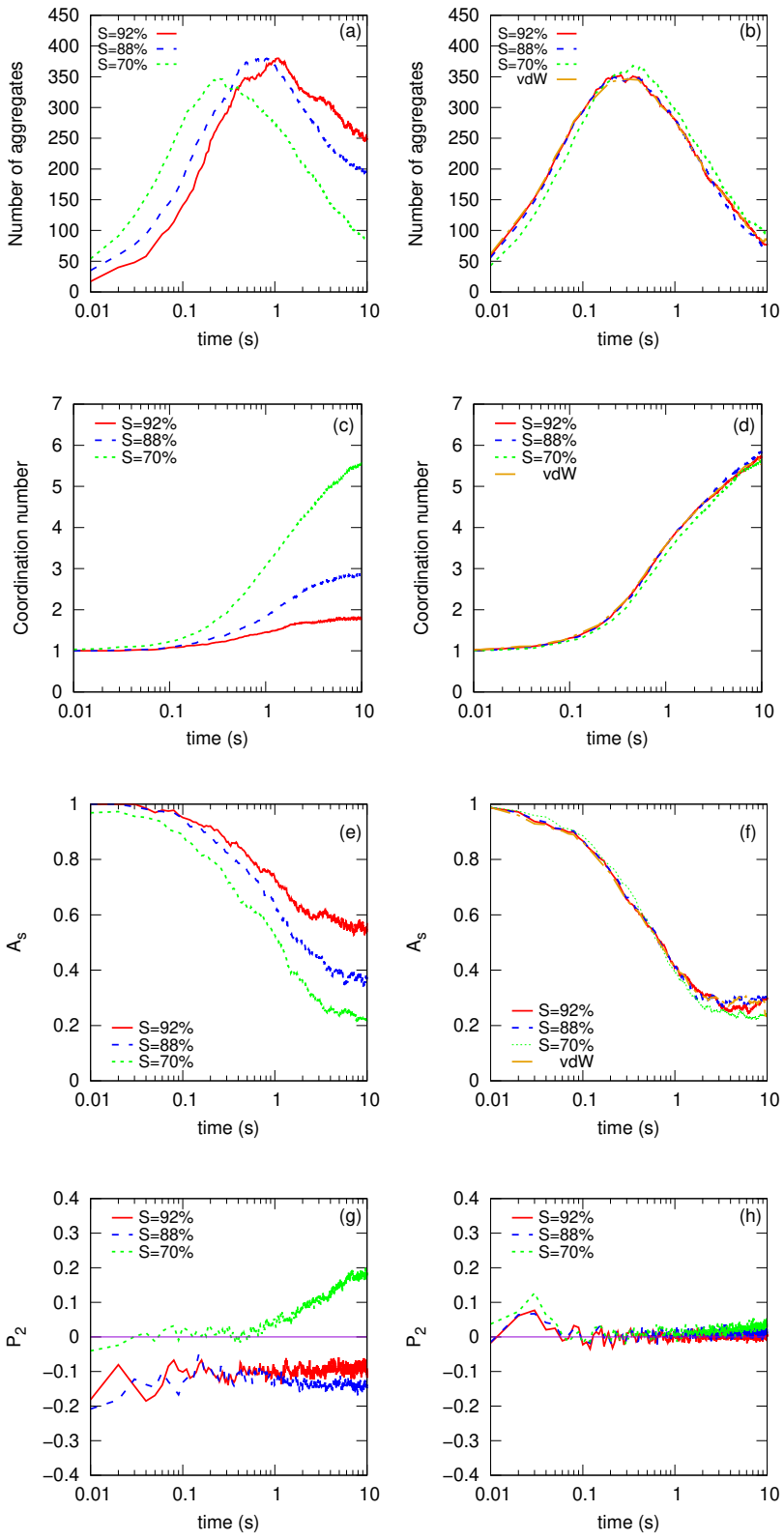

Figure 6: Characterization of the aggregation in the Brownian dynamics simulations performed for different sizes of the silica modified part ($S = 92\%$, $S = 88\%$ and $S = 70\%$) and for uniform particles interacting only via van der Waals attractions ($S = 100\%$ at pH_n): number of aggregates for pH_a (a) and pH_n (b); evolution of the coordination number for pH_a (c) and pH_n (d); evolution of the asphericity parameter (A_s) for pH_a (e) and pH_n (f) and evolution of P_2 for pH_a (g) and pH_n (h).

is also observed that this kinetics is similar to the kinetics observed in the simulation where particles only experience van der Waals attraction. At this pH, the modified parts of Janus particles are not charged and aggregation is mainly due to van der Waals interactions between them. For all values of S, aggregates are compact with a coordination number around 6, and they have an asphericity around 0.25 (see Figures 6d and 6f). Fractal dimensions are found at $D_f = 1.74 \pm 0.04$, 1.72 ± 0.04 and 1.81 ± 0.04 for $S = 92\%$, 88% and 70% respectively. It is also observed that particles are randomly oriented in the aggregates unlike at pH_a (see Figures 6h and 5). All these results show that for pH_n, the S value has little influence on the structure of the aggregates in contrast to pH_a. This can be explained by the interactions between the different parts of the Janus particles. As already mentioned, the dominant interaction in this system is that of van der Waals, and the electrostatic repulsions between the unmodified patches have little influence, especially because they are small in size.

In order to compare more quantitatively the experimental and numerical results, we analyzed more precisely the number of coordination in 2D. From the confocal microscopy pictures, we identified the coordinates of the particles within the aggregates by locating the brightest pixel at the center of each green spot. From these coordinates, the average coordination number was determined in 2D by considering only the particles that do not interpenetrate more than 2 pixels, i.e. 170 nm, to take into account the error made on the position of the particles. Particles in the aggregate which interpenetrate more than this, are considered to be not on the same plane and are not included in the calculation. To perform the same type of analysis in simulations, the simulation boxes were cut in one direction every µm, which is the depth analyzed in confocal microscopy. The coordinates of the particles located in this cut were projected on the same plane, and the analysis of the mean coordination number was obtained by considering only the particles that do not overlap as in experiments. This method was chosen because it allows not to take into account the particles which are located below a lower plane and which are not visible in microscopy. The results obtained are reported in the Table 2. At pH_a, the experimental and numerical results show the same trend. Coordination increases as S decreases. At pH_n, little change in coordination is observed with S. However, these results show how it is difficult to compare simulations and experiments more quantitatively. Several factors of uncertainty may indeed explain these differences. Microscopic analyses can only be carried out on aggregates where the particles are well distinguished, i.e.

	S=92%		S=88%		S=70%	
	simulation	experiments	simulation	experiments	simulation	experiments
pH_a	1.9 ± 0.2	2.3 ±0.8	2.6 ±0.3	3.2 ±0.4	4.1 ±0.9	3.7 ±0.4
pH_n	3.6 ±0.8	2.9 ±0.3	3.6 ±1.0	3.4 ± 0.7	4.0±0.8	3.3 ±0.5

Table 2: 2D coordination number measured in simulation and in experiments (in experiments averages are done over a range comprised between 145 and 300 particles).

on small aggregates where few particles are superimposed. Very compact aggregates cannot therefore be analyzed. In addition, the synthesis method makes it possible to obtain a large number of Janus particles, but the exact definition of the modified surface area is not very precise, contrary to that used in simulation. However, qualitatively, the behaviour observed in simulation is consistent with that observed experimentally. In Figure 2, for $S = 72\%$ at pH_a, aggregates seem more compact compared to the aggregates obtained with $S = 100\%$ at pH_n, which is the more common aggregation in oxide suspensions. To see if the simulations could provide an explanation for this observation, complementary calculations have been performed until $t = 20\,s$ for $S = 70\%$ at pH_a and pH_n and for particles interacting only through van der Waals attractions (similar to $S = 100\%$ at pH_n). Snapshots of the simulations obtained at $t = 20\,s$ as well as the evolution of A_s are shown in Figure 7. After 10 s, it appears that A_s slightly increases in simulations where particles interact only with van der Waals interactions contrary to the Janus particles. In this case, aggregates are thus more elongated. Fractal dimensions measured at $D_f = 1.89 \pm 0.06$, 1.73±0.05 and 1.63± 0.05 for pH_a, pH_b and for the van der Waals interactions respectively, confirm this observation. From previous works, it is known that the shape of aggregates is explained by the competition between the kinetics of aggregate coalescence and the kinetics of aggregate reorganization [36]. Since the kinetics of aggregate coalescence is similar in the three simulations (at $t = 20\,s$, 54, 55 and 54 aggregates are found for pH_a, pH_b and for the van der Waals interactions respectively), this difference should be explained by the aggregate reorganization. Reorganization of the aggregates is indeed expected in order to maximize the number of contacts between the attractive parts of particles, which minimizes the potential energy and gives compact configurations. The reorganization kinetics has been assessed by following the reorganization of an isolated aggregate obtained just after the coalescence of two small aggregates (see

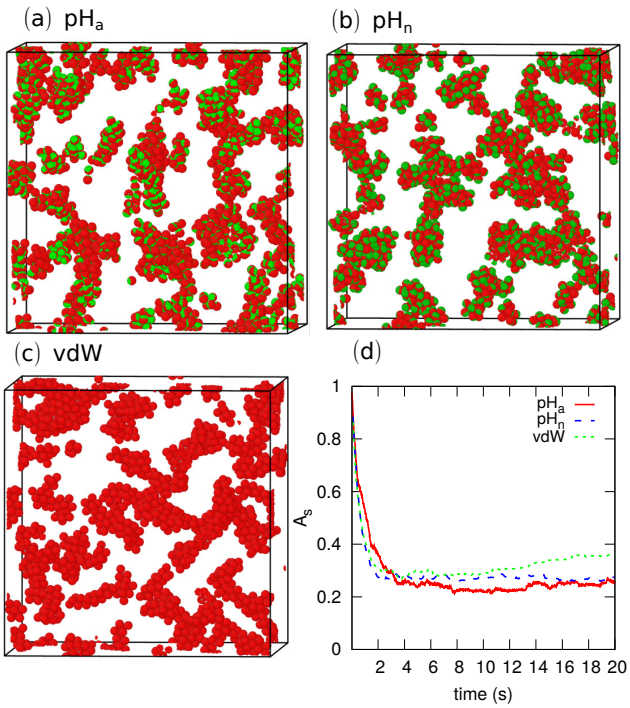

Figure 7: Snapshots of simulations obtained at $t = 20\,\mathrm{s}$: (a) $S = 70\%$ at pH$_a$, (b) $S = 70\%$ at pH$_n$ and (c) $S = 100\%$ at pH$_n$ (particles interact only via van der Waals interactions). (d) Evolution of the asphericity as a function of time: pH$_a$ ($S = 70\%$ at pH$_a$), pH$_n$ ($S = 70\%$ at pH$_n$) and vdW($S = 100\%$ at pH$_n$).

Figure 8). The reorganization has been characterized by the asphericity A_s and the mean coordination number of aggregated particles as a function of time (see Figure 9). It should be noted that, after 1 s, asphericity and coordination no longer evolves in the case of the aggregate of particles interacting via van der Waals, whereas for the Janus particles a continuous reorganization of the aggregates is observed. Indeed, for Janus particles, A_s as well as the averaged coordination number vary all along the simulations. The coordination number sometimes decreases, which corresponds to the dissociation of particles and promotes the aggregate reorganization. Indeed, the coordination overall increases reflecting the aggregate reorganization in a more compact shape. Bochicchio *et al.* have shown that long dissociation times (e.g. $\approx 150\,\mathrm{s}$) prevent from the aggregate reorganization leading to "branched" aggregates, whereas short ones (e.g. $\approx 0.3\,\mathrm{s}$) allow an important aggregate reorganization leading to compact, even crystallized aggregates in Brownian dynamics simulations [37]. In previous simulations, the dissociation time of two aggregated patchy particles with S in the range [60;70]% was measured at around 3 s [24]. This value is low and may explain an important aggregate reorganization in the Janus particles simulations. The relatively easy dissociation

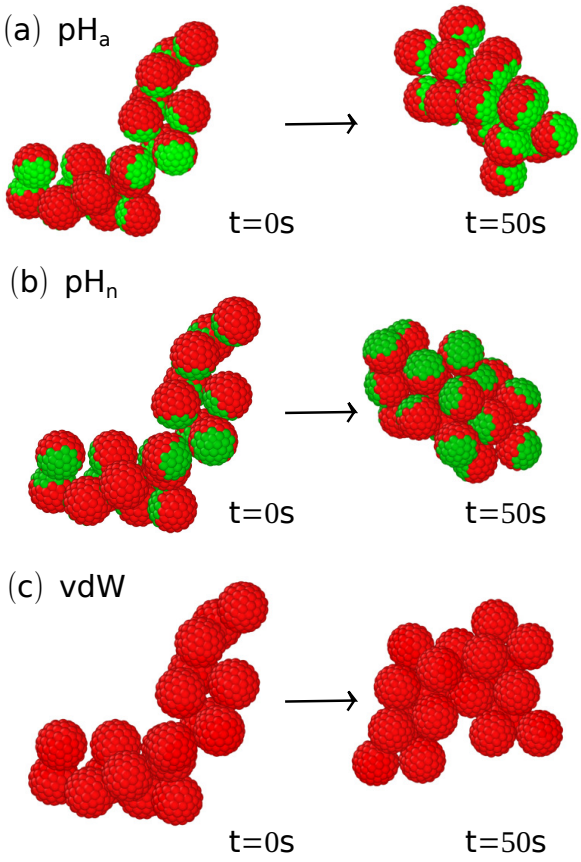

Figure 8: Snapshots of simulations performed on an isolated aggregate: (a) $S = 70\%$ at pH$_a$, (b) $S = 70\%$ at pH$_n$ and (c) $S = 100\%$ at pH$_n$ (particles interact only via van der Waals interactions).

of the Janus particles is due to repulsions between some parts of the particles. Thus, in the present simulations, when particles interact only via van der Waals interactions, the reorganization is slow and this leads to elongated aggregates. On the contrary, Janus particles aggregates can be reorganized much more easily to maximize the contact number between the attractive parts, leading to more compact aggregates.

5. Conclusion

Silica-based charged Janus particles have been synthesized with patches of different sizes. Their aggregation in suspension was studied both experimentally and numerically at different pH. The simulation method used, based on a discretization of the surface properties of the particles, has been shown to be able to correctly predict both the aggregation tendency and the structure of the aggregates. The aggregates may have a wide range of shape and internal structure depending on both pH and patch size. In particular, Janus particles can form

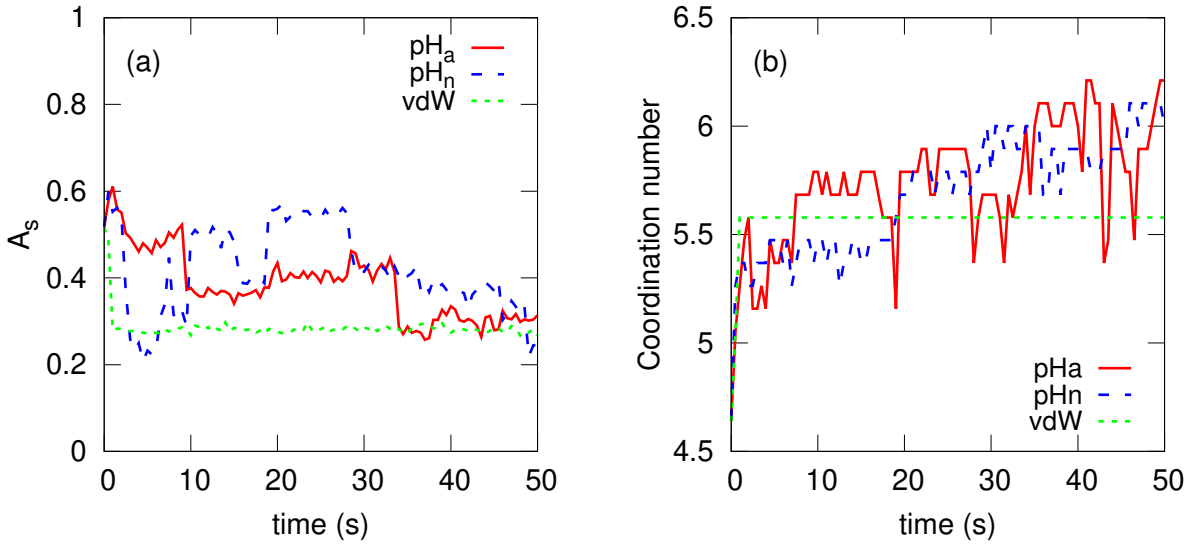

Figure 9: Evolution of the asphericity (a) and of the avergaed coordination number (b) performed on an isolated aggregate: pHa ($S = 70\%$ at pH_a), pHn ($S = 70\%$ at pH_n) and vdW($S = 100\%$ at pH_n).

aggregates of a compactness rarely equalled for isotropic particles.

A tricky point in numerically reproducing the experimentally observed aggregation behavior is the definition of the surface properties of each of the two parts of the Janus particles. The surface electric potential of the unmodified parts is assimilated to the experimentally measured zeta potential for the synthesized silica. The surface potential of the modified parts is estimated from the zeta potential measured for the Janus particles, the size of the patch (i.e. the unmodified part) and its surface potential. The detailed study of the behaviour in these Brownian dynamics simulations based on experimental considerations allows a better understanding of the aggregation mechanisms of the Janus particles.

The aggregation of charged Janus particles has already been studied numerically in literature, notably at the equilibrium [34, 35, 38, 39], but the number of studies remains limited compared to the number of studies carried out on amphiphilic particles. For charged Janus particles, patch size has been shown to have a large influence on the structure of the aggregates. When particles have small patches, aggregates tend to have elongated shapes [34, 35], which is also found experimentally and numerically in this study at pH_a. When the patch sizes are close to or equal to the size of the hemisphere, at equilibrium, compact aggregates are obtained. This was observed numerically and experimentally on small clusters by Hong *et al.* [14]. However, equilibrium studies are not sufficient in all cases to understand the struc-

ture of the experimentally observed large clusters and kinetic factors must be considered. In heteroaggregated suspensions, for example, equilibrium aggregates are compact; however, branched aggregates are experimentally observed, which is explained by the competition between coalescence and reorganization kinetics [40]. Here, by coupling both experimental observations and Brownian dynamics simulations, we prove that large compact aggregates, which correspond to the equilibrium structures, can be obtained in experiments. This is explained by rapid local reorganizations, favoured by a very likely particle detachment due to the presence of patches of opposite charges.

Moreover, in this study, a wide range of pH is investigated to account for the aggregation in suspensions not only when the two parts of the Janus particles are oppositely charged but also when one of them is weakly charged, which is rarely described in the literature, but may also be of interest for applications in the field of materials.

All these results show that the aggregation of the silica-based synthesized Janus particles can be controlled by changing both the proportion of the modified part of the particles and the pH. Such particles can be used to obtain either elongated or compact aggregates in which the particles may have a preferential orientation. These structures are interesting and the use of such particles should be considered to produce new ceramic materials with a specific microstructure.

Acknowledgments

The authors thank the Région Nouvelle-Aquitaine for its financial support. The authors thank also CALI and its team for providing the computational facilities (CALI has been financed by the region Limousin, the institutes XLIM, IPAM, GEIST, and the University of Limoges). The authors also thank Claire Carrion for her help on the confocal microscope. Figures 3, 4, 5, 7, 8 have been obtained by Ovito [41].

[1] M. Zrinyi, Z. Hrvlgyi (Eds.), From Colloids to Nanotechnology, 2004th Edition, Springer, 2004.

[2] F. Li, D. P. Josephson, A. Stein, Colloidal assembly: The road from particles to colloidal molecules and crystals, Angewandte Chemie International Edition 50 (2) (2011) 360–388.

[3] D. Morphew, D. Chakrabarti, Clusters of anisotropic colloidal particles: From colloidal molecules to supracolloidal structures, Curr. Opin. Colloid Interface Sci. 30 (2017) 70 – 80.

[4] A. Perro, S. Reculusa, S. Ravaine, E. Bourgeat-Lami, E. Duguet, Design and synthesis of Janus micro- and nanoparticles, Journal of Materials Chemistry 15 (35-36) (2005) 3745–3760. doi:10.1039/B505099E.

[5] C. Kaewsaneha, P. Tangboriboonrat, D. Polpanich, M. Eissa, A. Elaissari, Preparation of Janus colloidal particles via Pickering emulsion: An overview, Colloids and Surfaces A: Physicochemical and Engineering Aspects 439 (Supplement C) (2013) 35–42. doi:10.1016/j.colsurfa.2013.01.004.

[6] L. Hong, S. Jiang, S. Granick, Simple Method to Produce Janus Colloidal Particles in Large Quantity, Langmuir 22 (23) (2006) 9495–9499. doi:10.1021/la062716z.

[7] S. Jiang, M. Schultz, Q. Chen, J. Moore, S. Granick, Solvent-free synthesis of Janus colloidal particles, Langmuir 24 (2008) 10073–10077. doi:https://doi.org/10.1021/la800895g.

[8] S. Jiang, S. Granick, Controlling the geometry (Janus balance) of amphiphilic colloidal particles, Langmuir 24 (2008) 2438–2445.

[9] A. Zenerino, C. Peyratout, A. Aimable, Synthesis of fluorinated ceramic Janus particles via a Pickering emulsion method, J. Colloid Interface Sci. 450 (2015) 174–181.

[10] X. Xu, Y. Liu, Y. Gao, H. Li, Preparation of Au@silica Janus nanosheets and their catalytic application, Colloids Surf., A 529 (2017) 613 – 620. doi:https://doi.org/10.1016/j.colsurfa.2017.06.048.

[11] K. Panwar, M. Jassal, A. Agrawal, TiO_2-SiO_2 Janus particles with highly enhanced photocatalytic activity, RSC Adv. 6 (2016) 92754–92764. doi:10.1039/C6RA12378C.

[12] E. Y. Hwang, J. S. Lee, D. W. Lim, Oppositely charged, stimuli-responsive anisotropic nanoparticles for colloidal self-assembly, Langmuir 35 (13) (2019) 4589–4602. doi:10.1021/acs.langmuir.8b04002.

[13] E. Y. Hwang, M. J. Kang, A. Basheer, D. W. Lim, Tunable decoupling of dual drug release of oppositely charged, stimuli-responsive anisotropic nanoparticles, ACS Applied Materials & Interfaces 12 (1) (2020) 135–150. doi:10.1021/acsami.9b15485.

[14] L. Hong, A. Cacciuto, E. Luitjen, S. Granick, Clusters of charged janus spheres, Nano Letters 6 (2006) 2510–2514.

[15] A. Bianchi, G. Kahl, C. Likos, Inverse patchy colloids: from microscopic description to mesoscopic coarse-graining, Soft Matter 7 (2011) 8313.

[16] A. Bianchi, P. van Oostrum, C. Likos, G. Kahl, Inverse patchy colloids: Synthesis, modeling and self-organization, Curr. Opin. Colloid Interface Sci. 30 (2017) 8–15.

[17] M. Piechowiak, A. Videcoq, F. Rossignol, C. Pagnoux, C. Carrion, M. Cerbelaud, R. Ferrando, Oppositely charged model ceramic colloids: Numerical predictions and experimental observations by confocal laser scanning microscopy, Langmuir 26 (2010) 12540–12547, DOI: 10.1021/la101027d.

[18] K. Lebdioua, A. Aimable, M. Cerbelaud, A. Videcoq, C. Peyratout, Influence of different surfactants on pickering emulsions stabilized by submicronic silica, J. Colloid Interface Sci. 520 (2018) 127–133, DOI: 10.1016/j.jcis.2018.03.019.

[19] N. Kamarudin, A. Jalil, S. Triwahyono, N. Salleh, A. Karim, R. Mukti, B. Hameed, A. Ahmad, Role of 3-aminopropyltriethoxysilane in the preparation of mesoporous silica nanoparticles for ibuprofen delivery: Effect on physicochemical properties, Microporous and Mesoporous Materials 180 (2013) 235 – 241.

[20] D. M. Schlipf, S. E. Rankin, B. L. Knutson, Selective external surface functionalization of large-pore silica materials capable of protein loading, Microporous and Mesoporous Materials 244 (2017) 199 – 207. doi:https://doi.org/10.1016/j.micromeso.2016.10.023.

[21] N. Nishiyama, K. Horie, T. Asakura, Adsorption behavior of a silane coupling agent onto a colloidal silica surface studied by 29si nmr spectroscopy, Journal of Colloid and Interface Science 129 (1989) 113 – 119.

[22] F. Cuoq, A. Masion, J. Labille, J. Rose, F. Ziarelli, B. Prelot, J.-Y. Bottero, Preparation of amino-functionalized silica in aqueous conditions, Applied Surface Science 266 (2013) 155–160.

[23] H. Schmidt, H. Scholze, A. Kaiser, Principles of hydrolysis and condensation reaction of alkoxysilanes, Journal of Non-crystalline Solids 63 (1984) 1–11.

[24] M. Cerbelaud, K. Lebdioua, C. T. Tran, B. Crespin, A. Aimable, A. Videcoq, Brownian dynamics simulations of one-patch inverse patchy particles, Phys. Chem. Chem. Phys. 21 (2019) 23447–23458. doi:10.1039/C9CP04247D.

[25] B. Derjaguin, L. Landau, Theory of the stability of strongly charged lyophobic sols and of the adhesion of strongly charged particles in solution of electrolytes., Acta Physicochim. URSS 14 (1941) 633–662, DOI: 10.1016/0079–6816(93)90013–L.

[26] E. Verwey, J. Overbeek, Theory of the Stability of Lyophobic Colloids, Elsevier, Amsterdam, 1948.

[27] L. Bergström, Hamaker constants for inorganic materials, Adv. Colloid Interface Sci. 70 (1997) 125–169–A163.

[28] R. Hogg, T. Healy, D. Fuerstenau, Trans. Fraday Soc. 62 (1966) 1638–1651.

[29] C. T. Tran, B. Crespin, M. Cerbelaud, A. Videcoq, Brownian dynamics simulation on the GPU: Virtual colloidal suspensions, in: F. Jaillet, F. Zara, G. Zachmann (Eds.), Workshop on Virtual Reality Interaction and Physical Simulation, The Eurographics Association, 2015. doi:10.2312/vriphys.20151332.

[30] W. Russel, D. Saville, W. Schowalter, Colloidal Dispersions, Cambridge University Press: Cambridge, England, 1989.

[31] P.-Y. Hsiao, Chain morphology, swelling exponent, persistence length, like-charge attraction, and charge distribution around a chain in polyelectrolyte solutions: Effects of salt concentration and ion size studied by molecular dynamics simulations, Macromolecules 39 (2006) 7125–7137.

[32] A. Das, P.-Y. Hsiao, Charged dendrimers in trivalent salt solutions under the action of dc electric fields, J. Phys. Chem.B 118 (2014) 6265–6276.

[33] D. J. Beltran-Villegas, B. A. Schultz, N. H. P. Nguyen, S. C. Glotzer, R. G. Larson, Phase behavior of janus colloids determined by sedimentation equilibrium, Soft Matter 10 (2014) 4593–4602. doi:10.1039/C3SM53136H.

[34] M. Sabapathy, R. Mathews, E. Mani, Self-assembly of inverse patchy colloids with tunable patch coverage, Phys. Chem. Chem. Phys. 19 (2017) 13122–13132.

[35] J. Dempster, M. O. de la Cruz, Aggregation of heterogeneously charged colloids, ACS Nano 10 (2016) 5909–5915.

[36] M. Cerbelaud, A. Videcoq, P. Abélard, C. Pagnoux, F. Rossignol, R. Ferrando, Self-assembly of oppositely charged particles in dilute ceramic suspensions: predictive role of simulations, Soft Matter 6 (2009) 370–382.

[37] D. Bochicchio, A. Videcoq, A. Studart, R. Ferrando, Compact and ordered colloidal clusters from assemblydisassembly cycles: A numerical study, Journal of Colloid and Interface Science 440 (2015) 198 – 203.

[38] M. Hagy, R. Hernandez, Dynamical simulation of polar janus colloids: Equilibrium structure and thermodynamics, J. Chem. Phys. 137 (2012) 044505.

[39] E. Locatelli, E. Bianchi, Tuning the order of colloidal monolayers: assembly of heterogeneously charged colloids close to a patterned surface, Soft Matter 14 (2018) 8119–8136.

[40] M. Cerbelaud, A. Videcoq, R. Ferrando, Simulation of heteroaggregation in a suspension of alumina and silica particles: effect of dilution, J. Chem. Phys. 132 (2010) 084701.

[41] A. Stukowski, Visualization and analysis of atomistic simulation data with OVITO-the Open Visualization Tool, Modelling and simulations in materials science and Engineering 18. doi:10.1088/0965-0393/18/1/015012.

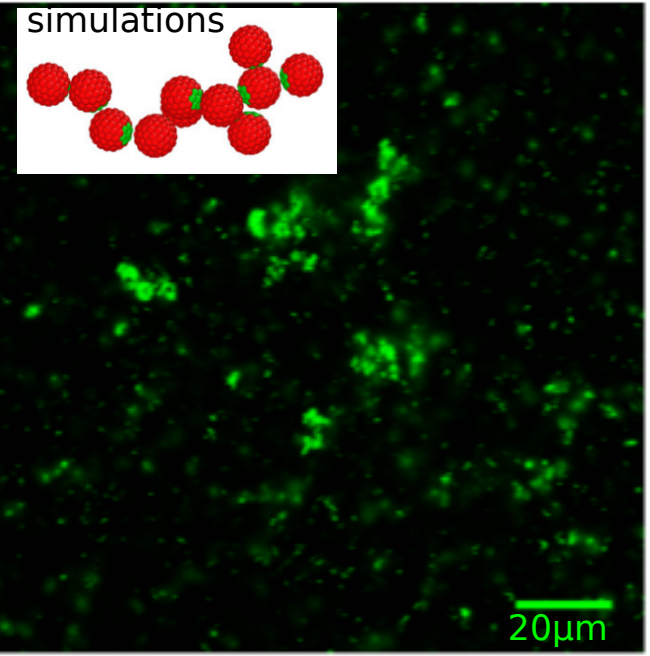

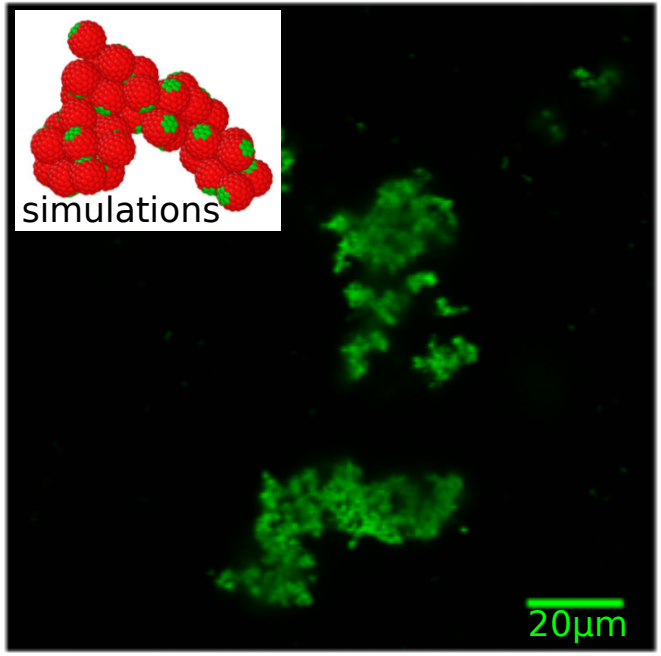

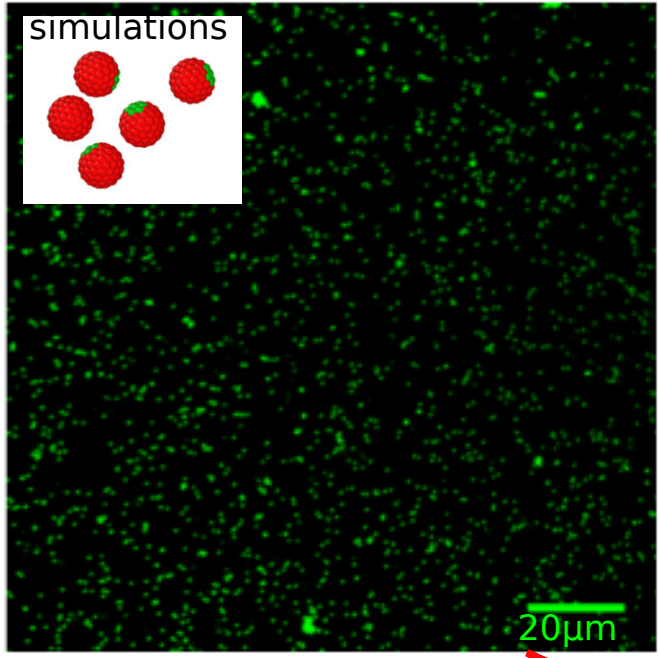

Increase of pH